

Voxel-based population analysis for correlating local dose and rectal toxicity in prostate cancer radiotherapy

This article has been downloaded from IOPscience. Please scroll down to see the full text article.

2013 Phys. Med. Biol. 58 2581

(<http://iopscience.iop.org/0031-9155/58/8/2581>)

View [the table of contents for this issue](#), or go to the [journal homepage](#) for more

Download details:

IP Address: 129.20.25.4

The article was downloaded on 27/03/2013 at 10:05

Please note that [terms and conditions apply](#).

Voxel-based population analysis for correlating local dose and rectal toxicity in prostate cancer radiotherapy

Oscar Acosta^{1,2}, Gael Drean^{1,2}, Juan D Ospina^{1,2}, Antoine Simon^{1,2},
Pascal Haigron^{1,2}, Caroline Lafond^{1,2,3} and Renaud de Crevoisier^{1,2,3}

¹ INSERM, U1099, Rennes, F-35000, France

² Université de Rennes 1, LTSI, Rennes, F-35000, France

³ Département de Radiothérapie, Centre Eugène Marquis, Rennes, F-35000, France

E-mail: oscar.acosta@univ-rennes1.fr


Received 30 November 2012, in final form 21 February 2013

Published 26 March 2013

Online at stacks.iop.org/PMB/58/2581

Abstract

The majority of current models utilized for predicting toxicity in prostate cancer radiotherapy are based on dose–volume histograms. One of their main drawbacks is the lack of spatial accuracy, since they consider the organs as a whole volume and thus ignore the heterogeneous intra-organ radiosensitivity. In this paper, we propose a dose-image-based framework to reveal the relationships between local dose and toxicity. In this approach, the three-dimensional (3D) planned dose distributions across a population are non-rigidly registered into a common coordinate system and compared at a voxel level, therefore enabling the identification of 3D anatomical patterns, which may be responsible for toxicity, at least to some extent. Additionally, different metrics were employed in order to assess the quality of the dose mapping. The value of this approach was demonstrated by prospectively analyzing rectal bleeding (\geq Grade 1 at 2 years) according to the CTCAE v3.0 classification in a series of 105 patients receiving 80 Gy to the prostate by intensity modulated radiation therapy (IMRT). Within the patients presenting bleeding, a significant dose excess (6 Gy on average, $p < 0.01$) was found in a region of the anterior rectal wall. This region, close to the prostate (1 cm), represented less than 10% of the rectum. This promising voxel-wise approach allowed subregions to be defined within the organ that may be involved in toxicity and, as such, must be considered during the inverse IMRT planning step.

 Online supplementary data available from stacks.iop.org/PMB/58/2581/mmedia

(Some figures may appear in colour only in the online journal)

1. Introduction

Radiation therapy (RT) is a commonly used efficacious treatment for prostate cancer (PC). Several strategies have been developed in order to improve local control, particularly by increasing the radiation dose with highly conformal techniques, suggesting a strong dose–effect relationship (Zietman *et al* 2010). Nowadays, the precision of treatment delivery is steadily improving due to the combination of intensity modulated RT (IMRT) and image-guided RT (IGRT). Hence the possibilities for achieving better control by increasing the dose are within reach. However, dose escalation is limited by rectal and urinary toxicity (Fonteyne *et al* 2008, Fiorino *et al* 2009a). Thus, the new competencies of the delivery systems could be efficiently exploited following adapted planning provided that accurate predictive toxicity models are available. The understanding of dose–volume versus toxicity relationships, therefore, becomes crucial for selecting appropriate constraints at the inverse planning step in IMRT.

The prediction of complications resulting from the irradiation has been extensively treated in the literature (Fiorino *et al* 2009a). These predictions are commonly based on the planned dose distribution via the dose–volume histograms (DVH) (Ting *et al* 1997) using radiobiological normal tissue complication probability (NTCP) models (Jensen *et al* 2010, Cambria *et al* 2009, Grigorov *et al* 2006, Wachter *et al* 2001). In the case of prostate cancer RT, different studies have shown a reproducible correlation between dose, volume, and rectal toxicity (Benk *et al* 1993, Fiorino *et al* 2002, Sohn *et al* 2007, Marzi *et al* 2007, Rancati *et al* 2004, Fiorino *et al* 2009b, Peeters *et al* 2006). However, current DVH-based models for toxicity prediction exhibit several limitations. Firstly, they do not implicitly integrate the subject's individual specificities, such as medical history, or concomitant treatments, such as chemotherapy or androgen deprivation, in their formulation. These patient-specific parameters have been considered but by stratifying the population (Fiorino *et al* 2008) at the expense of statistical power. Secondly, these models lack spatial accuracy, as they are not able to correlate the treatment outcome with the spatial dose distribution, thereby considering the organs as having homogeneous radio-sensitivity. Hence, the subtle potential correlation between local dose and toxicity may not be detected when the rich three-dimensional (3D) dose distribution is represented as a single organ DVH. The loss of local information may be aggravated when the DVH is further reduced to a single value such as the effective dose (D_{eff}) or equivalent uniform dose (EUD), which has also been shown to be correlated with the risk of toxicity (Schwarz *et al* 2004, Rancati *et al* 2004). Under these assumptions, depicting the relationship between local dose and toxicity is expected to be very informative, as it may be instrumental in identifying subregions at a higher risk of damage and thus facilitate the definition of more accurate dose–organ constraints.

The notion of spatial local dose variability and its relationship with toxicity have been already addressed in a limited number of works (Kupchak *et al* 2008), either using a parametric description of the dose distribution (Buettner *et al* 2009, 2011) or, for the first time, a voxel-based approach (Heemsbergen *et al* 2010, Witte *et al* 2010), although with approximations in terms of both anatomical matching and dose mapping. In these two voxel-wise studies, which were focused on urinary tract toxicity (Heemsbergen *et al* 2010) and prostate tumor control (Witte *et al* 2010), the dose mapping was mainly based on the radially-computed distances from the organ delineations. These results provided the way forward for complex voxel-based toxicity models based on more accurate inter-individual matching. In order for voxel-wise comparisons to be meaningful, the doses must be accurately mapped to a common coordinate system (CS), which is a challenging task due to the difficulties related to high inter-individual variability.

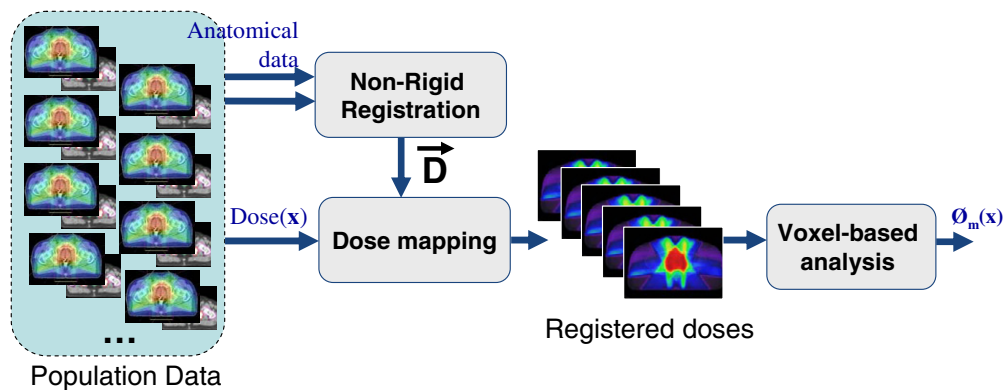


Figure 1. General framework of the proposed dose mapping and voxel-wise analysis. The anatomical information from a patient is NRR registered to a common template. The result is a vector field \vec{D} , which is used later on for dose mapping.

In response to the lack of spatial information of DVH-based predictive models, this paper proposes a new framework allowing the underlying relationship between local dose and toxicity to be analyzed across a population. This approach permits the identification of subregions within the critical organs, which may present a higher risk of damage and likely be responsible for toxicity. As depicted in figure 1, the proposed framework combines a precise anatomical non-rigid registration approach for mapping the population 3D dose distributions to a single CS and a voxel-wise analysis with respect to toxicity. The proposed model yields a 3D map $\Phi(x)$, $x \in \mathbb{R}^3$, which may be seen as a 3D NTCP cartography, depicting regions where the dose differences between two groups are statistically significant.

2. Materials and methods

The main steps of the method are described in figure 1: (i) the inter-individual CT and contour delineations are non-rigidly registered (NRR) into a common CS (common template) using organ-to-organ constraints; (ii) the planned dose distributions are mapped to the template by applying the computed transformations (dense deformation field \vec{D}); (iii) voxel-wise comparison of the mapped doses is performed (in this work, two-sampled *t*-tests for hypothesis testing). The resulting 3D images represent the dose differences between two groups and allow for the highlighting of voxels where those differences are statistically significant.

2.1. Patients, treatment and rectal toxicity

A total of 105 patients were included in the study, all having undergone IMRT for localized prostate cancer between July 2006 and June 2010 in the same institution. The target volume involved the prostate and seminal vesicles, without any lymph nodes. The total prescribed dose was 46 Gy to the seminal vesicles delivered in 4.6 weeks, and 80 Gy to the prostate delivered in 8 weeks, with a standard fractionation of 2 Gy/fraction. The whole treatment (patient positioning, CT acquisition, and volume delineations) and dose constraints complied with GETUG 06 recommendations, as previously reported (Beckendorf *et al* 2011). In particular, the constraints for the rectal wall were maximal dose ≤ 76 Gy and V72 Gy $\leq 25\%$. The size of the planning CT images in the axial plane was 512×512 pixels, with 1 mm image resolution

and 2 mm slice thickness. The used treatment planning system was Pinnacle V7.4 (Philips Medical System, Madison, WI). Each treatment plan used five field beams, in a step-and-shoot delivery configuration with gantry angles of 260°, 324°, 36°, 100° and 180°. The delivery was guided by means of an IGRT protocol, with cone beam CT images or two orthogonal images (kV or MV imaging devices), using gold fiducial markers in 57% of patients.

The median follow-up period was 38 months, with a minimum of 24 months for all patients. Rectal toxicity events were prospectively collected, as all of the patients participated in one of two randomized trials, either the GETUG 14 (testing the benefit of 4-month androgen deprivation in addition to receiving 80 Gy of radiation to the prostate) or the STIC-IGRT (testing the benefit of IGRT) (De Crevoisier *et al* 2009). Rectal toxicity was scored according to the common terminology criteria for adverse events (CTCAE) version 3.0. The endpoint of the study was 2-year Grade ≥ 1 rectal bleeding, excluding acute toxicity. Patients with a history of hemorrhoids were not allowed to be scored as Grade 1 bleeding. In total, 24 patients presented at least a Grade 1 rectal bleeding event, which occurred between 6 and 24 months following treatment.

2.2. Inter-individual registration and dose mapping

Three issues were addressed for mapping inter-individual 3D dose distributions to a single CS: (i) selection of the common CS (template); (ii) registration of the inter-individual anatomies; (iii) propagation of the individual dose distributions to the template.

2.2.1. Template selection. One question that arises when defining a common CS for population analysis is the computation of inter-individual similarities (Aljabar *et al* 2009, Wu *et al* 2007, Commowick and Malandain 2007). In order to diminish the bias inherent to using a single template, one potential strategy is to select a typical individual from the database, which is quite similar to the majority of individuals. Thus, intensity-based similarity metrics may define the distance between individuals (Aljabar *et al* 2009). Given an adequate inter-individual similarity, the strategy may further include a clustering step aimed to identify the average individual that best represents the population (Ramus and Malandain 2010).

In this study, a typical individual was selected from the database in order to define the template. This individual was found by affinity propagation clustering (Frey and Dueck 2007) among a subgroup of randomly selected patients from the whole database. During the clustering step, the template emerged as the exemplar, which represented the individual closest to all of the remaining individuals. The considered inter-individual similarity criteria were the sum of squared differences (SSD) computed after rigid registration between individuals I_K and I_L :

$$\text{SSD} = -\frac{1}{N} \sum_{x \in \Omega} |I_K(x) - I_L(x)|^2, \quad (1)$$

where N is the number of voxels x in the CT scans and Ω represents the pelvic region where the computation was performed. Figure 2 shows the selected template with delineated organs representation.

2.2.2. Registration. Registering inter-individual CTs is particularly challenging due to the poor soft-tissue contrast, large inter-individual variability and differences in bladder and rectum filling (Acosta *et al* 2011). Given this inter-individual anatomical matching, pure intensity-based registration was shown to be not accurate enough to meet the requirements for population analysis, possibly leading to non-negligible local errors (Drean *et al* 2011).

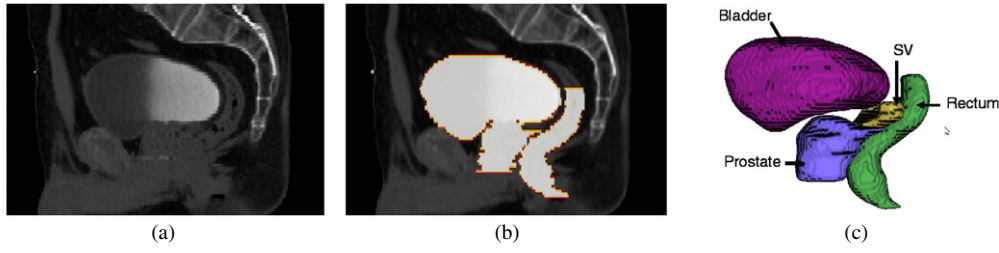


Figure 2. Selected template. Sagittal views of the (a) original CT scan, (b) the organ delineations and (c) 3D representation. The prostate, rectum, bladder and seminal vesicles (SV) are visible.

However, if all the complementary information pertaining to the individual's anatomy was used, the registration's performance would improve considerably. We propose herewith an organ-driven non-rigid registration strategy built from the demons algorithm (Thirion 1998), which yields an accurate match between organs in the common CS. This non-rigid registration approach advantageously exploits information available at the planning stage, namely the 3D anatomical data and organ delineations as summarized in figure 3 and detailed below.

Let I_k represent an individual to be registered in the template I_T : (i) for each individual's delineated organ $O_k = \{Prostate_k, Bladder_k, Rectum_k\}$ an Euclidean distance map $L(O_k)$ (Danielsson 1988) was first computed. Thus, each map $L_{O_k}(\mathbf{x})$ represented for each $\mathbf{x} \in \mathbb{R}^3$ within the organ, a distance to the O_k surface. Likewise for the counterpart in the template $O_T = \{Prostate_T, Bladder_T, Rectum_T\}$ and corresponding distance maps $L_{O_T}(\mathbf{x})$; (ii) each of the distance maps was mutually normalized, yielding a set of normalized distance maps as $NL_{O_k}(\mathbf{x}) = \max\{L_{O_T}(\mathbf{x})\} \cdot L_{O_k}(\mathbf{x})$ and $NL_{O_T}(\mathbf{x}) = \max\{L_{O_k}(\mathbf{x})\} \cdot L_{O_T}(\mathbf{x})$. (iii) The NL of both I_k and I_T were then superposed over the CT scans, replacing the original organ delineations; (iv) the demons algorithm (Thirion 1998) was finally used to non-rigidly register I_k to I_T . These NL_{O_k} constituted additional anatomic constraints, which facilitated the anatomic matching process. The use of Euclidean distance maps from organ surfaces reinforced accurate matching of doses close to the boundaries where pure intensity-based CT registration would fail. The result of this registration step was a dense deformation field $\vec{D}(x)$, which was then used to propagate the dose as shown in figure 4.

2.2.3. Dose propagation. The deformation field $\vec{D}(x)$, obtained in the previous step, is a set of 3D vectors defined at each voxel (figure 4), thereby providing a nonlinear transformation to be applied to the dose distributions.

The doses were eventually propagated into the template by applying $\vec{D}(x)$ to each voxel position $\in I_k$ and sampled again in the space of I_T using tri-linear interpolation. Figure 5 shows an example of dose propagated from an individual toward the template.

2.3. Scores for validation of registration and dose mapping

Different parameters were used in order to assess the quality of the dose mapping. These parameters validated both the accuracy of organ overlap after non-rigid registration as well as the coincidence of doses between the native and common CSs. Regarding registration, the Dice similarity coefficient (DSC) and Hausdorff distance (H) were used. The DSC (Zijdenbos *et al* 1994) is defined as

$$DSC = 2 \left(\frac{|R_T \cap R_I|}{|R_T| + |R_I|} \right) \quad (2)$$

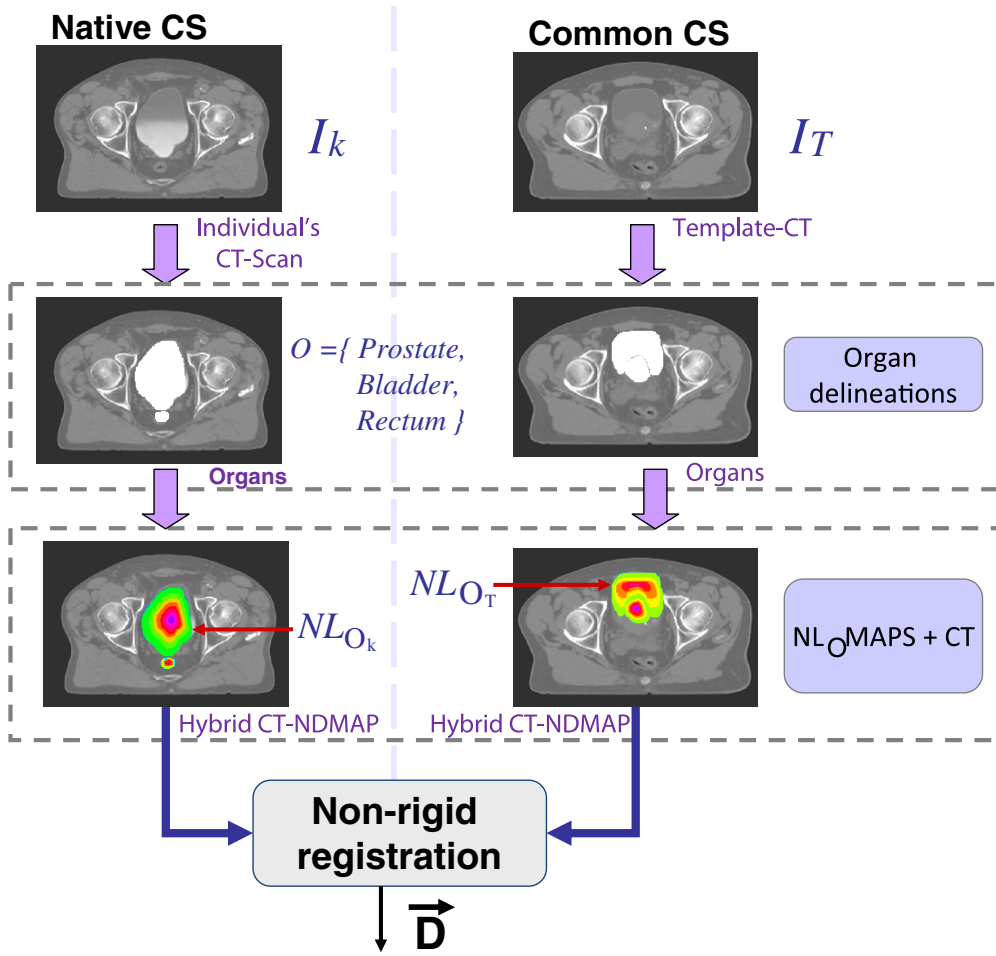


Figure 3. The hybrid non-rigid registration (NRR) approach, bringing 3D doses from their native coordinate system (CS) to the common CS. After organ delineation, normalized distance maps (NL_O MAPS) are computed and combined with the CT scan to be registered. The result is the transformation (deformation field) used to map the dose.

where \cap is the intersection between each individual's registered rectum R_I and the rectum of the template R_T . This score ranges from 0 to 1 as a function of the volume overlap.

The Hausdorff distance (Hausdorff 1918), implemented in Commandeur *et al* (2011)⁴ was used in order to compute the distance H between two sets of points or surfaces $S_1 = \{s1_1, \dots, s1_p\}$ and $S_2 = \{s2_1, \dots, s2_q\} \in \mathbb{R}^3$ as

$$H(S_1, S_2) = \max\{h(S_1, S_2), h(S_2, S_1)\} \quad (3)$$

where

$$h(S_1, S_2) = \max_{s1 \in S_1} \min_{s2 \in S_2} \|s1 - s2\| \quad (4)$$

and $\|\cdot\|$ is the Euclidean distance between the S_1 and S_2 points. The calculation $h(S_1, S_2)$ identifies the point $s1 \in S_1$ that is farthest from any point of S_2 and measures the distance from

⁴ Open source available at: www.vtkjournal.org/browse/publication/839

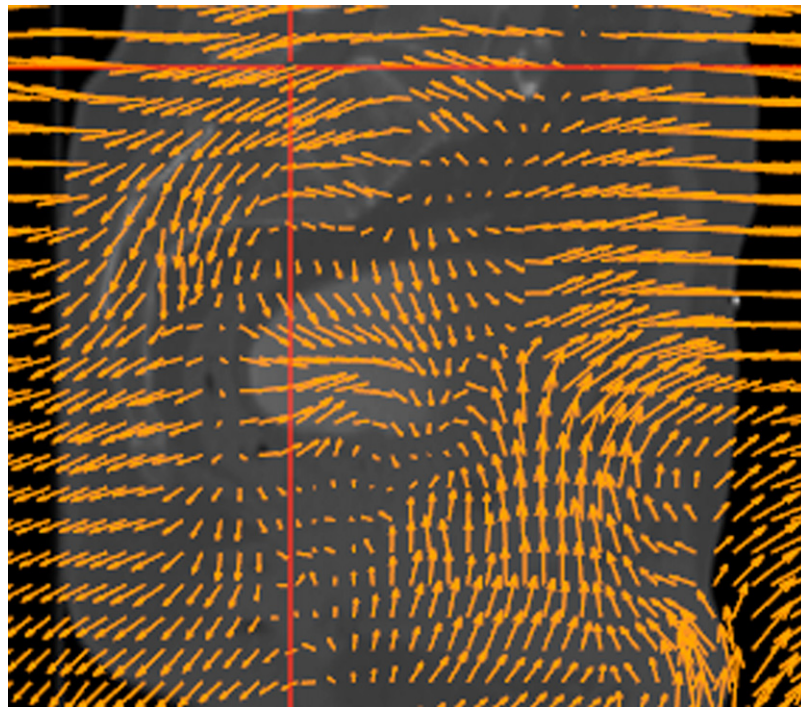


Figure 4. Example of the resulting transformation (deformation field, D) used to map the dose.

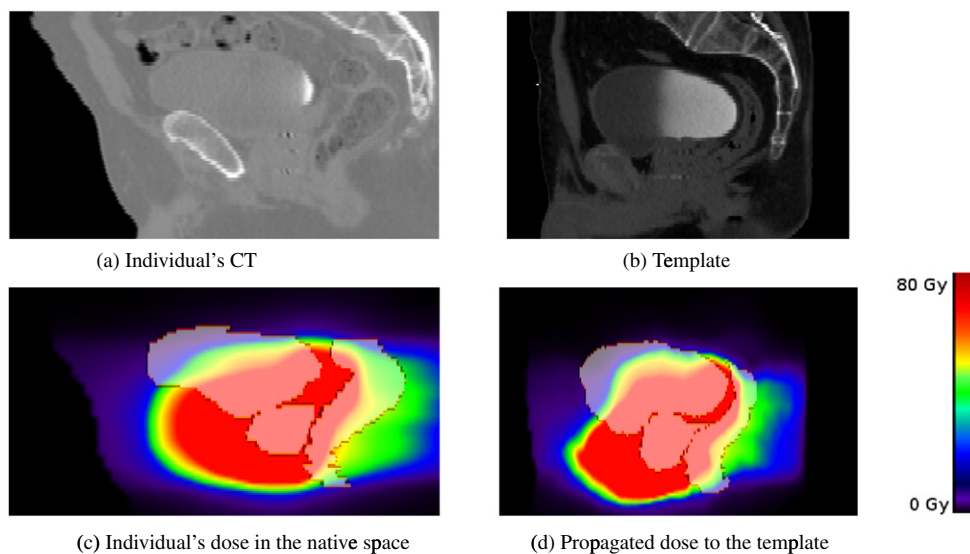


Figure 5. Example of 3D non-rigid dose mapping using the computed transformation from figure 4. (a) A typical individual's CT; (b) the template; (c) an individual's TPS planned dose in the native coordinate system; (d) dose mapped to the template coordinate system.

s_1 to its nearest neighbor in S_2 using $\| \cdot \|$. This means that $h(S_1, S_2)$ ranks each point of S_1 based on its distance to the nearest point of S_2 , and then uses the largest ranked point as the distance (Huttenlocher *et al* 1993).

For the validation of dose coincidence between native and common spaces, in order to compare dose mapping accuracy, we implemented two scores pertaining to the relative difference of areas (RDA) of DVHs and dose–organ overlap (DOO).

The RDA assesses the differences in DVHs following dose mapping while considering the information in the template CS. For a given individual, let h_1 be the DVH computed between the mapped dose and the NRR rectum, and let h_2 be the DVH computed with the warped dose and the rectum of the template,

$$\text{RDA}(h_1, h_2) = \frac{\int_0^{\text{dose}_{\max}} |h_1 - h_2| \, du}{\max \left\{ \int_0^{\text{dose}_{\max}} h_1 \, du, \int_0^{\text{dose}_{\max}} h_2 \, du \right\}}. \quad (5)$$

The RDA is normalized between 0 (when $h_1 = h_2$) and 1 using the area under the DVH curve. The DVHs are expected to be preserved following registration. Therefore, if RDA tends to zero, a DVH-based NTCP model would be similar, whether computed in the native space or the common CSs.

The DOO is a score that measures the coincidence of both the organs and dose distribution in the common space following registration. This parameter is computed as follows:

$$\text{DOO}(\text{dose}, R_I, R_T) = \frac{\int_{R_I \cap R_T} \text{dose}(x) \, dx}{\int_{R_I \cup R_T} \text{dose}(x) \, dx}, \quad (6)$$

where $\text{dose}(x)$ is the registered dose distributions at x , computed on the union and intersection of both organs (template R_T and registered R_I). The DOO penalizes the overlap errors within the higher gradients of dose. Conversely, if the overlap is measured in a region of homogeneous dose, the score is the same as the Jaccard similarity metric (JAC), namely:

$$\text{JAC} = \left(\frac{R_T \cap R_I}{R_T \cup R_I} \right) \quad (7)$$

where \cup represents the union of both R_T and R_I . Hence, the DOO ranges between 0 and 1, attaining the highest value when the dose on each voxel of both organs is the same.

2.4. Voxel-based analysis

Statistical voxel-based comparisons are instrumental in detecting regional changes between groups by locally computing the difference of a signal across a given population (Friston *et al* 1995, Friston *et al* 2006). Different examples were reported in the literature, such as voxel-based morphometry (Ashburner and Friston 2000), which allow the differences related to density changes in a given tissue, such as gray matter changes in the brain on account of a disease, to be assessed (Abbott *et al* 2012, Kakeda and Korogi 2010). These differences may reflect local anatomical changes, such as tensor-based morphometry (Hua *et al* 2008, Leow *et al* 2007), the analysis of which relies on Jacobian images obtained by warping individual data to a common template. Some studies have combined hypometabolism and atrophy using positron emission tomography images, where the differences may be accounted for by functional integrity (Chételat *et al* 2008, Desgranges *et al* 2007).

In our study, the signals to be compared on a voxel level were the 3D planned dose distributions across the population. Two groups were therefore constituted, namely individuals with rectal bleeding versus those with no rectal bleeding, according to the inclusion criteria described in section 2.1. In order for the voxel-wise comparisons to be meaningful, only accurately registered rectum data was included. Registration accuracy was measured as a high-volume overlap (dice score >0.7) between the rectum in template space and NRR individuals. As a result, two groups were obtained, comprising 51 non-bleeding and 12 bleeding subjects,

Table 1. Characterization of the statistically significant voxels ($p < 0.01$), R1, with respect to the distance to the prostate-seminal vesicle (PSV) surface: % of the whole significant region (R1) and mean dose difference.

Rectal distance from PSV surface (mm)	% of R1	Averaged dose difference (Gy)
5	35.86	4.55
10	97.28	6.32
15	98.97	6.43
20	98.97	6.43
30	98.97	6.43

respectively. Voxel-wise two-sampled t -tests were performed, resulting in 3D maps for both dose differences and p -values. The regions exhibiting statistically significant between-group differences ($p < 0.01$) were characterized in terms of absolute volume, mean dose difference, and rectal localization in the rectum, more precisely distance of the region to the prostate and seminal vesicle surfaces.

3. Results

Figure 5 depicts an example of the dose mapping from the individual's native CS to the template CS using the proposed framework.

Considering the whole population, the average dice score for the rectum was 0.75 ± 0.12 and the Hausdorff distance $28.17 \text{ mm} \pm 16$, while the DOO and the RDA were 0.64 ± 0.1 and 0.09 ± 0.05 , respectively.

Figure 6(a) depicts the between-group dose differences in the rectum. The dose prescribed to patients with rectal bleeding was significantly higher (6.43 Gy, $p < 0.01$) in a small portion of the rectum (labeled R1). Figures 6(b) and (c) show lateral and coronal views of the 3D reconstructed common template highlighting the region R1. This 3184.06 mm^3 region, located in the anterior wall and middle-third of the rectum, represented 9.11% of the total rectal volume.

Table 1 characterizes the distribution of statistically significant voxels (region R1) with respect to the distance to the prostate and seminal vesicles surfaces. 35.86% of R1 was within the first 5 mm, receiving in average 4.55 Gy more within the rectal bleeding patients but more than 90% of R1 was located within the first centimeter (anterior wall). This result shows that the more sensitive area was within the first 10 to 15 mm, and that within this region, the average dose delivered to rectal bleeding patients was exceeded by +6.40 Gy as compared to that delivered to non-bleeding patients.

Figure 7 shows the averaged DVHs within R1, compared with the DVHs computed for the whole rectum. Inside R1, the differences between bleeding and non-bleeding patients were between $V_{40}\text{Gy}$ and $V_{66}\text{Gy}$, reaching statistical significance ($p < 0.01$), as opposed to the whole rectum where no significant differences were found.

4. Discussion

The particular novelty presented here, in comparison with traditional DVH-based models, makes maximal use of 3D dose distributions, resulting in a correlation between local toxicity and local planned dose. The proposed method relies on an accurate non-rigid registration strategy allowing the dose distributions across a population to be mapped and compared on a common CS. The voxel-wise analysis would permit the identification of subregions

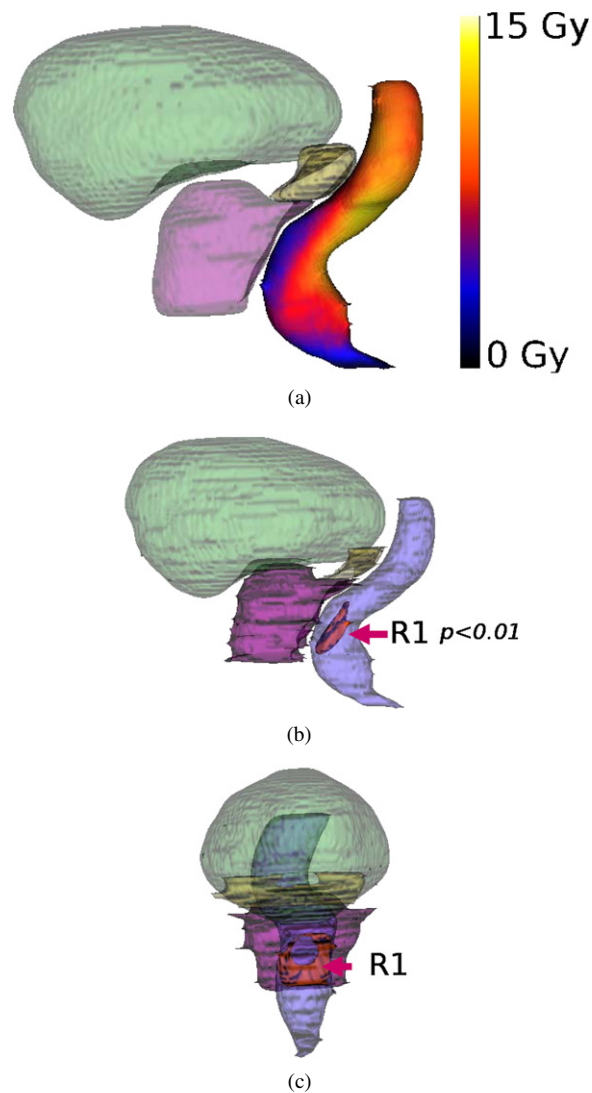


Figure 6. Results of voxel-wise analysis in the template space for rectal bleeding. (a) Mean differences in dose between the two groups. (b), (c) Three-dimensional reconstruction of lateral and coronal views of the common template, highlighting the rectal region R1, where these differences were statistically significant ($p < 0.01$). In our study, this region represented less than 10% of the whole rectum and appears close to the prostate in the anterior rectal wall. (see supplementary data at stacks.iop.org/PMB/58/2581/mmedia).

within the organs at risk, which may be responsible for secondary effects, hence highlighting heterogeneous intra-organ radio-sensitivity.

The Grade ≥ 1 bleeding toxicity was chosen as the main endpoint in this study, as such events are relatively frequent when high-dose is delivered to the prostate (approximately 20% after two years) allowing for statistical tests to be performed. In addition, rectal bleeding is a symptom that can be relatively objectively reported (excluding patients with a history of hemorrhoids). Moreover, most of the studies assessing NTCP models for rectal toxicity are focused on rectal bleeding.

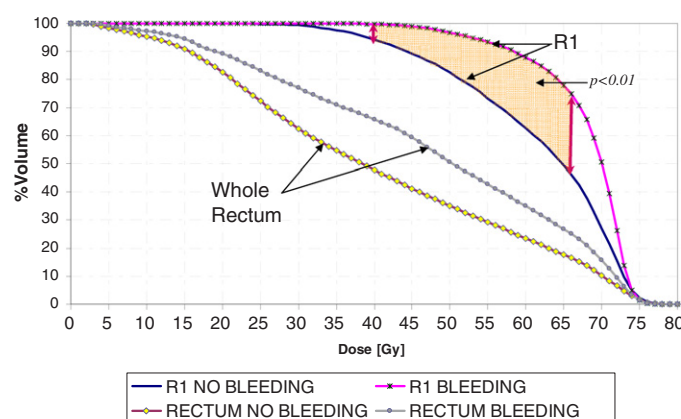


Figure 7. Averaged dose–volume histogram comparison for the two groups. They were computed in the rectum and in R1. In addition, the DVHs in R1 were significantly different (p -values < 0.01) for R1 between V_{40} and V_{66} .

Based on our results, the anterior part of the rectal wall correlated with rectal bleeding. This region, representing less than 10% of the whole rectum, was given 6 Gy more, on average, in bleeding patients and was mainly located within the first 15 mm, close to where high-dose was delivered to the prostate. In addition, the average DVH computed within this region allowed for better separation between both groups, resulting in a clear volume effect (figure 7).

These results are in line with the Lyman–Kutcher–Burman NTCP model studies, which reported effective volume values (often denoted by n) between 0.06 and 0.13 for moderate/severe bleeding, thus highlighting the high-dose range impact and suggesting that the rectum was a prevalently serial organ. Indeed, in our study, a small non circumferential volume within the anterior part of the rectum was found to be correlated with rectal bleeding (Grade ≥ 1). However, the ‘intermediate’ doses inside this rectal region better discriminate bleeders from non-bleeders, as it is discussed in Rancati *et al* (2004). Nevertheless, results from the literature as well as from our voxel-based comparison study must be interpreted with caution, taking into account several RT parameters. These results depend on the ability of the conformal technique to spare the posterior part of the rectum from ‘intermediate’ dose levels (40 to 50 Gy), total dose prescribed in the prostate, and dose volume constraints in the rectum, potentially allowing a high-dose to be delivered to the anterior rectal wall. The observation that the anterior part of the rectum appears to be involved in rectal bleeding equally corresponds to the clinical experience of rectal cauterization. This finding is in line with a report on a series of 44 patients who voluntarily accepted to undergo flexible rectosigmoidoscopy. In this investigation, the occurrence of telangiectasia increased from the posterior to the anterior rectal wall, and Grade 3 telangiectasia was exclusively limited to the high-dose region of the anterior rectal wall (Wachter *et al* 2000).

Nevertheless, it should be noted that the toxicity results must be carefully considered in terms of cause–effect relationships. We are depicting regions that are correlated with toxicity, which are not necessarily responsible for it. New cohorts of patients are required in order to validate the hypothesis raised by means of this voxel-based approach. New findings in terms of dose–toxicity relationships may appear for other symptoms. Larger series of patients would allow for a multivariate analysis to be performed, taking into account patient-specific characteristics in addition to the treatment parameters. Other organs should also be explored, such as the bladder, where most of the models have not found any dose–effect relationship.

Another key point to take into account is the potential difference between the planned and actual delivered doses. In effect, in the course of the treatment, the organs at risk may deform or displace with respect to the initial conditions at the planning step. This is also an issue for the current NTCP models that consider only planned dose distributions. In our study, however, more than half of the included patients were treated following an IGRT protocol, which likely minimizes the impact of anatomical variations, at least to some extent. The next generation of NTCP models should ideally be established on both planning imaging, as well as imaging acquired during each fraction. This issue is currently being tackled in further works, where dose-tracking strategies may help improve accuracy. In addition, statistical approaches are being developed so as to model these uncertainties (Söhn *et al* 2005), considering the actual delivered dose as a random variable, while investigating the impact of the deformations on toxicity outcome.

The proposed framework, as depicted in figure 1, relies on a non-rigid matching of organs and CT scans. The use of Euclidean distance maps from organ boundaries allowed for accurate matching of doses close to the rectal wall. Additionally, further registration approaches are being investigated to improve the aligning of different structures. A combined CT-organ registration with a spatial weighted function was recently proposed (Drean *et al* 2012), but still needs to be validated within this framework.

Another point to be investigated in future research is the optimal template selection. Different strategies exist to select a template from a database to be representative of a given population. In some applications, an average individual may be obtained by iteratively registering and computing intensity means (Rohlfing *et al* 2004). Other approaches are based on group-wise registration (Wachinger and Navab 2012). In our clustering strategy, we selected a single representative individual, however, more clusters may also be selected in order to reproduce the voxel-wise analysis on different templates (Rohlfing *et al* 2009). The question brought to mind is therefore the computation of inter-individual similarities, which may be tackled, as already done in the past within the scope of atlas based segmentation (Rohlfing *et al* 2004, Wu *et al* 2007).

Concerning the voxel-based statistical dose analysis, we are considering other alternative approaches that take into account the effect of individuals, in line with the non-parametric mixed-effect model proposed by Ospina *et al* (2011, 2012). This method, which exploits intra-individual spatial correlation at each voxel location, can handle more efficiently large variances between groups. Preliminary results demonstrated an improved sensitivity and reliability for group analysis, as compared with standard voxel-wise methods. One interesting feature is the possibility of including clinical data or other confounding variables within the formulation. A similar method that is currently being explored is the dimensionality reduction of data (Chen *et al* 2011) in order to extract the main spatial features of the 3D dose distributions, which would allow patients to be classified in two groups.

Determining the heterogeneous intra-organ sensitivity across a population, combined with patient-specific information in an inverse IMRT planning, may allow for the production of personalized treatment with high local control and reduced toxicity, as observed in other studies with different constraints (Söhn *et al* 2007). This general scope may be extended in order to adapt ongoing treatment, thus taking into account not only data from a model but also integrating the dynamic individual specificities (i.e. tumor response and anatomical modifications). To achieve a more accurate prediction in inverse adaptive planning, further work should also consider the inclusion of the individual's clinical variables that may be involved in toxicity (age and concomitant treatments, etc).

Within this perspective for adaptive radiotherapy, the set of parameters Φ extracted from the population data may be then combined with the individual's parameters $\phi_p(t)$, which may

change during the treatment in order to better adapt the therapy. In practice, a comparison between equivalent treatment plans could be performed, allowing the best treatment i.e. the treatment that spares the more sensitive regions, to be selected during therapy.

5. Conclusion

In this work, we have proposed a methodological framework based on non-rigid registration aimed at determining the local dose–effect relationship in prostate cancer radiotherapy, helping reveal the heterogeneous intra-organ radio-sensitivity to predict toxicity. It is based on a non-rigid registration scheme combining organ delineations with CT scans and thus enabling better organ matching among individuals. Our contribution exploits information available at the planning stage, namely the 3D anatomical data, 3D organ delineations, and planned doses. This study opens the door for new methods of analyzing toxicity with increased accuracy, which may eventually lead to improved constraints within IMRT planning.

References

- Abbott D F, Pell G S, Pardoe H R and Jackson G D 2012 Selecting appropriate voxel-based methods for neuroimaging studies *NeuroImage* **59** 885–6
- Acosta O, Simon A, Monge F, Commandeur F, Bassirou C, Cazoulat G, de Crevoisier R and Haigron P 2011 Evaluation of multi-atlas-based segmentation of CT scans in prostate cancer radiotherapy *IEEE Int. Symp. on Biomedical Imaging: From Nano to Macro* pp 1966–69
- Aljabar P, Heckemann R, Hammers A, Hajnal J and Rueckert D 2009 Multi-atlas based segmentation of brain images: atlas selection and its effect on accuracy *NeuroImage* **46** 726–38
- Ashburner J and Friston K 2000 Voxel-based morphometry—the methods *NeuroImage* **11** 805–21
- Beckendorf V *et al* 2011 70 Gy versus 80 Gy in localized prostate cancer: 5-year results of GETUG 06 randomized trial *Int. J. Radiat. Oncol. Biol. Phys.* **80** 1056–63
- Benk V A, Adams J A, Shipley W U, Urie M M, McManus P L, Efid J T, Willett C G and Goitein M 1993 Late rectal bleeding following combined x-ray and proton high dose irradiation for patients with stages T3–T4 prostate carcinoma *Int. J. Radiat. Oncol. Biol. Phys.* **26** 551–7
- Buettner F, Gulliford S L, Webb S and Partridge M 2011 Modeling late rectal toxicities based on a parameterized representation of the 3D dose distribution *Phys. Med. Biol.* **56** 2103
- Buettner F, Gulliford S L, Webb S, Sydes M R, Dearnaley D P and Partridge M 2009 Assessing correlations between the spatial distribution of the dose to the rectal wall and late rectal toxicity after prostate radiotherapy: an analysis of data from the MRC RT01 trial (ISRCTN 47772397) *Phys. Med. Biol.* **54** 6535
- Cambria R, Jereczek-Fossa B A, Cattani F, Garibaldi C, Zerini D, Fodor C, Serafini F, Pedrolì G and Orecchia R 2009 Evaluation of late rectal toxicity after conformal radiotherapy for prostate cancer: a comparison between dose–volume constraints and NTCP use *Strahlenther. Onkol.* **185** 384–9
- Chen B, Acosta O, Kachenoura A, Ospina J, Drèan G, Simon A, Bellanger J-J, Haigron P and de Crevoisier R 2011 Spatial characterization and classification of rectal bleeding in prostate cancer radiotherapy with a voxel-based principal components analysis model for 3D dose distribution *Prostate Cancer Imaging. Image Analysis and Image-Guided Interventions (Lecture Notes in Computer Science* vol 6963) ed A Madabhushi, J Dowling, H Huisman and D Barratt (Berlin: Springer) pp 60–69
- Chételat G, Desgranges B, Landeau B, Mézenge F, Poline J B, de la Sayette V, Viader F, Eustache F and Baron J-C 2008 Direct voxel-based comparison between grey matter hypometabolism and atrophy in Alzheimer's disease *Brain* **131** 60–71
- Commandeur F, Velut J and Acosta O 2011 A VTK algorithm for the computation of the Hausdorff distance *VTK J.* **839** (<http://hdl.handle.net/10380/3322>)
- Commowick O and Malandain G 2007 Efficient selection of the most similar image in a database for critical structures segmentation *MICCAI '07: 10th Int. Conf. on Medical Image Computing and Computer-Assisted Intervention* vol 4792 pp 203–10
- Danielsson P-E 1980 Euclidean distance mapping *Comput. Graph. Image Process.* **14** 227–48
- de Crevoisier R, Pommier P, Bachaud J, Crehange G, Boutry C, Chauvet B, Nguyen T, Laplanche A, Aubelle M and Lagrange J 2009 Image-guided radiation therapy (IGRT) in prostate cancer: preliminary results in prostate registration and acute toxicity of a randomized study *Int. J. Radiat. Oncol. Biol. Phys.* **75** (Suppl. 3) S99

- Desgranges B, Matuszewski V, Piolino P, Chételat G, Mézenge F, Landeau B, de la Sayette V, Belliard S and Eustache F 2007 Anatomical and functional alterations in semantic dementia: a voxel-based MRI and PET study *Neurobiol. Aging* **28** 1904–13
- Drean G, Acosta O, Simon A, de Crevoisier R and Haigron P 2011 Evaluation of inter-individual pelvic CT-scans registration *IRBM* **32** 288–92
- Drean G, Acosta O, Simon A, de Crevoisier R and Haigron P 2012 Inter-individual organ-driven CT registration for dose mapping in prostate cancer radiotherapy *ISBI'12: 9th IEEE Int. Symp. on Biomedical Imaging* pp 370–73
- Fiorino C, Cozzarini C, Vavassori V, Sanguineti G, Bianchi C, Cattaneo G M, Foppiano F, Magli A and Piazzolla A 2002 Relationships between DVHs and late rectal bleeding after radiotherapy for prostate cancer: analysis of a large group of patients pooled from three institutions *Radiother. Oncol.* **64** 1–12
- Fiorino C *et al* 2008 Clinical and dosimetric predictors of late rectal syndrome after 3D-CRT for localized prostate cancer: preliminary results of a multicenter prospective study *Int. J. Radiat. Oncol. Biol. Phys.* **70** 1130–7
- Fiorino C, Rancati T and Valdagni R 2009a Predictive models of toxicity in external radiotherapy: dosimetric issues *Cancer* **115** (Suppl. 13) 3135–40
- Fiorino C, Valdagni R, Rancati T and Sanguineti G 2009b Dose–volume effects for normal tissues in external radiotherapy: pelvis *Radiother. Oncol.* **93** 153–67
- Fonteyne V, Villeirs G, Speleers B, Neve W D, Wagter C D, Lumen N and Meerleer G D 2008 Intensity-modulated radiotherapy as primary therapy for prostate cancer: report on acute toxicity after dose escalation with simultaneous integrated boost to intraprostatic lesion *Int. J. Radiat. Oncol. Biol. Phys.* **72** 799–807
- Frey B J and Dueck D 2007 Clustering by passing messages between data points *Science* **315** 972–6
- Friston K J, Ashburner J T, Kiebel S, Nichols T and Penny W D (ed) 2006 *Statistical Parametric Mapping: The Analysis of Functional Brain Images* (London: Academic)
- Friston K J, Holmes A P, Worsley K J, Poline J P, Frith C D and Frackowiak R S J 1995 Statistical parametric maps in functional imaging: a general linear approach *Human Brain Mapping* **2** 189–210
- Grigorov G N, Chow J C L, Grigorov L, Jiang R and Barnett R B 2006 IMRT: improvement in treatment planning efficiency using NTCP calculation independent of the dose–volume–histogram *Med. Phys.* **33** 1250–8
- Hausdorff F 1918 Dimension und äußeres maß *Math. Ann.* **79** 157–79
- Heemsbergen W D, Al-Mamgani A, Witte M G, van Herk M, Pos F J and Lebesque J V 2010 Urinary obstruction in prostate cancer patients from the Dutch trial (68 Gy versus 78 Gy): relationships with local dose, acute effects, and baseline characteristics *Int. J. Radiat. Oncol. Biol. Phys.* **78** 19–25
- Hua X, Leow A D, Parikshak N, Lee S, Chiang M-C, Toga A W, Jack C R, Weiner M W, Thompson P M and N Initiative A D 2008 Tensor-based morphometry as a neuroimaging biomarker for Alzheimer's disease: an MRI study of 676 AD, MCI, and normal subjects *NeuroImage* **43** 458–69
- Huttenlocher D P, Klandermans G A and Rucklidge W J 1993 Comparing images using the Hausdorff distance *IEEE Trans. Pattern Anal. Mach. Intell.* **15** 850–6
- Jensen I, Carl J, Lund B, Larsen E H and Nielsen J 2010 Radiobiological impact of reduced margins and treatment technique for prostate cancer in terms of tumor control probability (TCP) and normal tissue complication probability (NTCP) *Med. Dosim.* **36** 130–7
- Kakeda S and Korogi Y 2010 The efficacy of a voxel-based morphometry on the analysis of imaging in schizophrenia, temporal lobe epilepsy, and Alzheimer's disease/mild cognitive impairment: a review *Neuroradiology* **52** 711–21
- Kupchak C, Battista J and Dyk J V 2008 Experience-driven dose–volume histogram maps of NTCP risk as an aid for radiation treatment plan selection and optimization *Med. Phys.* **35** 333–43
- Leow A, Yanovsky I, Chiang M-C, Lee A, Klunder A, Lu A, Becker J, Davis S, Toga A and Thompson P 2007 Statistical properties of Jacobian maps and the realization of unbiased large-deformation nonlinear image registration *IEEE Trans. Med. Imaging* **26** 822–32
- Marzi S, Arcangeli G, Saracino B, Petrongari M G, Bruzzaniti V, Iaccarino G, Landoni V, Soriani A and Benassi M 2007 Relationships between rectal wall dose–volume constraints and radiobiologic indices of toxicity for patients with prostate cancer *Int. J. Radiat. Oncol. Biol. Phys.* **68** 41–9
- Ospina J D, Acosta O, Drèan G, Cazoulat G, Simon A, Correa J C, Haigron P and de Crevoisier R 2011 Spatial nonparametric mixed-effects model with spatial-varying coefficients for analysis of populations *Machine Learning in Medical Imaging (Lecture Notes in Computer Science* vol 7009) ed K Suzuki, F Wang, Shen D and P Yan (Berlin: Springer) pp 142–50
- Ospina J, Benquet P, Correa J and Acosta O 2012 A mixed effects spatio temporal model to assess the joint effect of ageing and Alzheimer's disease in gray matter volume *MICCAI-NIBAD '12: Workshop on Novel Imaging Biomarkers for Alzheimer's Disease and Related Disorders* pp 190–7

- Peeters S T H, Hoogeman M S, Heemsbergen W D, Hart A A M, Koper P C M and Lebesque J V 2006 Rectal bleeding, fecal incontinence, and high stool frequency after conformal radiotherapy for prostate cancer: normal tissue complication probability modeling *Int. J. Radiat. Oncol. Biol. Phys.* **66** 11–19
- Ramus L and Malandain G 2010 Assessing selection methods in the context of multi-atlas based segmentation *IEEE Int. Symp. on Biomedical Imaging: From Nano to Macro* pp 1321–24
- Rancati T *et al* 2004 Fitting late rectal bleeding data using different NTCP models: results from an italian multi-centric study (AIROPROS0101) *Radiother. Oncol.* **73** 21–32
- Rohlfing T, Brandt R, Menzel R and Maurer C R 2004 Evaluation of atlas selection strategies for atlas-based image segmentation with application to confocal microscopy images of bee brains *NeuroImage* **21** 1428–42
- Rohlfing T, Sullivan E V and Pfefferbaum A 2009 Subject-matched templates for spatial normalization *Med. Image Comput. Assist. Interv.* **12** 224–31
- Schwarz M, Lebesque J V, Mijneer B J and Damen E M 2004 Sensitivity of treatment plan optimisation for prostate cancer using the equivalent uniform dose (EUD) with respect to the rectal wall volume parameter *Radiother. Oncol.* **73** 209–18
- Sohn M, Alber M and Yan D 2007 Principal component analysis-based pattern analysis of dose–volume histograms and influence on rectal toxicity *Int. J. Radiat. Oncol. Biol. Phys.* **69** 230–9
- Söhn M, Birkner M, Yan D and Alber M 2005 Modelling individual geometric variation based on dominant eigenmodes of organ deformation: implementation and evaluation *Phys. Med. Biol.* **50** 5893–908
- Söhn M, Yan D, Liang J, Meldolesi E, Vargas C and Alber M 2007 Incidence of late rectal bleeding in high-dose conformal radiotherapy of prostate cancer using equivalent uniform dose-based and dose–volume-based normal tissue complication probability models *Int. J. Radiat. Oncol. Biol. Phys.* **67** 1066–73
- Thirion J-P 1998 Image matching as a diffusion process: an analogy with Maxwell's demons *Med. Image Anal.* **2** 243–60
- Ting J Y, Wu X, Fiedler J A, Yang C, Watzich M L and Markoe A 1997 Dose–volume histograms for bladder and rectum *Int. J. Radiat. Oncol. Biol. Phys.* **38** 1105–11
- Wachinger C and Navab N 2012 Simultaneous registration of multiple images: similarity metrics and efficient optimization *IEEE Trans. Pattern Anal. Mach. Intell.* at press (doi: [10.1109/TPAMI.2012.196](https://doi.org/10.1109/TPAMI.2012.196))
- Wachter S, Gerstner N, Goldner G, Pötzi R, Wambersie A and Pötter R 2000 Endoscopic scoring of late rectal mucosal damage after conformal radiotherapy for prostatic carcinoma *Radiother. Oncol.* **54** 11–19
- Wachter S, Gerstner N, Goldner G, Pötzi R, Wambersie A and Pötter R 2001 Rectal sequelae after conformal radiotherapy of prostate cancer: dose–volume histograms as predictive factors *Radiother. Oncol.* **59** 65–70
- Witte M G, Heemsbergen W D, Bohoslavsky R, Pos F J, Al-Mamgani A, Lebesque J V and van Herk M 2010 Relating dose outside the prostate with freedom from failure in the Dutch trial 68 Gy versus 78 Gy *Int. J. Radiat. Oncol. Biol. Phys.* **77** 131–8
- Wu M, Rosano C, Lopez-Garcia P, Carter C S and Aizenstein H J 2007 Optimum template selection for atlas-based segmentation *NeuroImage* **34** 1612–8
- Zietman A L *et al* 2010 Randomized trial comparing conventional-dose with high-dose conformal radiation therapy in early-stage adenocarcinoma of the prostate: long-term results from Proton Radiation Oncology Group/American College of Radiology 95-09 *J. Clin. Oncol.* **28** 1106–11
- Zijdenbos A P, Dawant B M, Margolin R A and Palmer A C 1994 Morphometric analysis of white matter lesions in MR images: method and validation *IEEE Trans. Med. Imaging* **13** 716–24